Tissue Clearing and Its Application to Bone and Dental Tissues

D. Jing[1,2], Y. Yi[1,2], W. Luo[1], S. Zhang[2], Q. Yuan[2], J. Wang[2], E. Lachika[3], Z. Zhao[2], and H. Zhao[1]

Abstract

Opaqueness of animal tissue can be attributed mostly to light absorption and light scattering. In most noncleared tissue samples, confocal images can be acquired at no more than a 100-µm depth. Tissue-clearing techniques have emerged in recent years in the neuroscience field. Many tissue-clearing methods have been developed, and they all follow similar working principles. During the tissue-clearing process, chemical or physical treatments are applied to remove components blocking or scattering the light. Finally, samples are immersed in a designated clearing medium to achieve a uniform refractive index and to gain transparency. Once the transparency is reached, images can be acquired even at several millimeters of depth with high resolution. Tissue clearing has become an essential tool for neuroscientists to investigate the neural connectome or to analyze spatial information of various types of brain cells. Other than neural science research, tissue-clearing techniques also have applications for bone research. Several methods have been developed for clearing bones. Clearing treatment enables 3-dimensional imaging of bones without sectioning and provides important new insights that are difficult or impossible to acquire with conventional approaches. Application of tissue-clearing technique on dental research remains limited. This review will provide an overview of the recent literature related to the methods and application of various tissue-clearing methods. The following aspects will be covered: general principles for the tissue-clearing technique, current available methods for clearing bones and teeth, general principles of 3-dimensional imaging acquisition and data processing, applications of tissue clearing on studying biological processes within bones and teeth, and future directions for 3-dimensional imaging.

Keywords: digital imaging, periodontal ligament, microscopy, dental pulp biology, bone biology, dental implant

Introduction

Tissue-clearing (TC) techniques provide a new tool for 3-dimensional (3-D) imaging by turning tissues transparent. The first TC technique was developed in 1914 (Spalteholz 1914) and was reintroduced into the neuroscience community nearly a century later (Steinke and Wolff 2001). In recent decades, various TC techniques have been developed by neuroscientists for visualizing neural connections within the brain or spinal cord. In 2015, a TC technique was first introduced into hard tissue research (Acar et al. 2015).

Tissue opaqueness is caused by light scattering and absorption. Light scattering can be attributed to refractive index (RI) nonconformity among different tissue components: water (RI ~1.33), protein (RI ~1.43), lipids (RI ~1.44), organelles (RI ~1.38 to 1.41), and inorganic mineral (RI ~1.55) (Seo et al. 2016). In addition, numerous colorized components, including heme, lipofuscin, and melanin, strongly absorb light (Susaki and Ueda 2016). To achieve transparency, chemical or physical treatments were applied to eliminate elements scattering or blocking the light. Finally, samples were immersed in designated medium to achieve uniform internal RI, named RI matching. Once the transparency was reached, high-quality images could be acquired even at several millimeters of depth.

Current TC methods can be classified into 3 major categories (Fig. 1):

1. Organic solvent-based TC techniques, such as BABB (Dodt et al. 2007), DISCO series (Erturk et al. 2012; Pan et al. 2016; Cai et al. 2019), Fluoclear BABB (Schwarz et al. 2015), ECi (Klingberg et al. 2017), and PEGASOS (Jing et al. 2018). The final RI matching clearing medium for these methods is nonaqueous

[1]Department of Restorative Sciences, School of Dentistry, Texas A&M University, Dallas, TX, USA
[2]State Key Laboratory of Oral Diseases and National Clinical Research Center for Oral Diseases, West China Hospital of Stomatology, Sichuan University, Chengdu, P.R. China
[3]Intelligent Imaging Innovations (3i), Denver, CO, USA

Corresponding Authors:
H. Zhao, Department of Restorative Sciences, School of Dentistry, Texas A&M University, 3302 Gaston Avenue, Dallas, TX 75246, USA.
Email: hzhao@tamhsc.edu
Z. Zhao, State Key Laboratory of Oral Diseases and National Clinical Research Center for Oral Diseases, West China Hospital of Stomatology, Sichuan University, No. 14, 3rd Section Renmin South Road, Chengdu 610041, P.R. China.
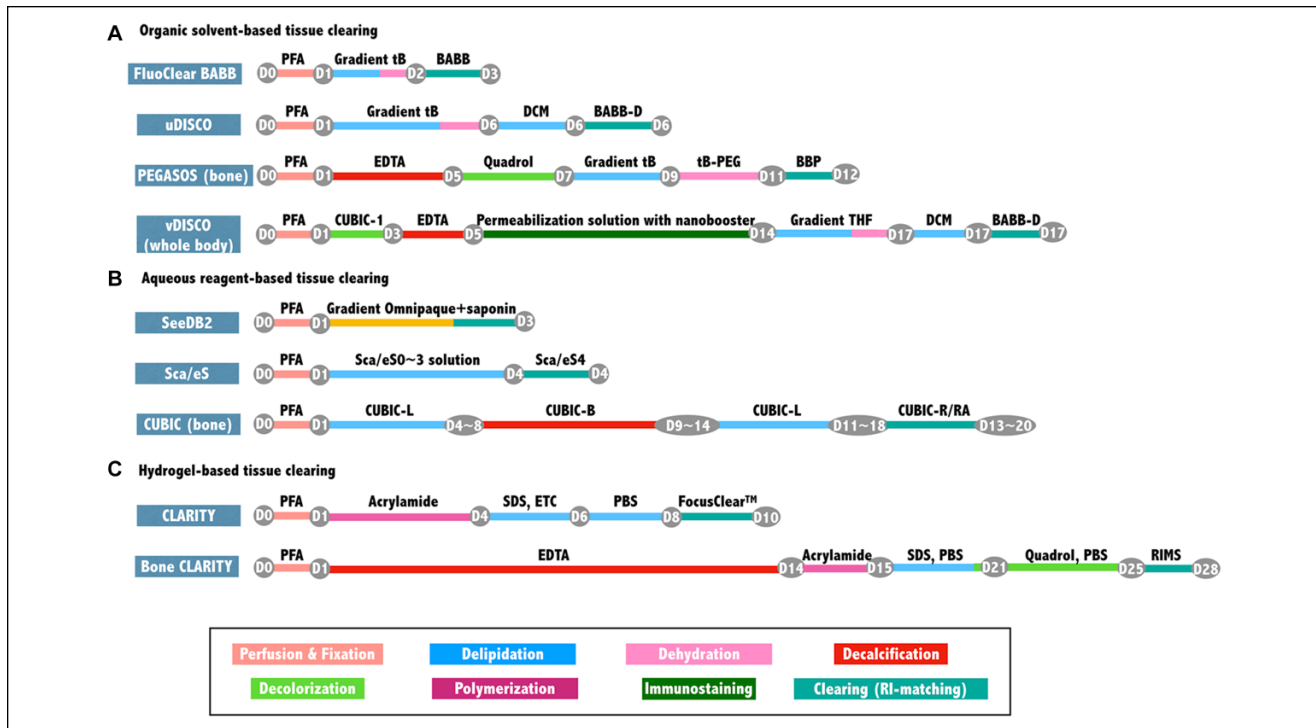Email: zhaozhihe@vip.163.com

Figure 1. Three major categories of tissue-clearing techniques and representative methods. Treatment steps and timetables for each clearing method are briefly described. Solvent-based methods include FluoClear BABB (Schwarz et al. 2015), uDISCO (Pan et al. 2016), PEGASOS (Jing et al. 2018), and vDISCO (Cai et al. 2019). Aqueous reagent-based methods include SeeDB2, Sca*l*eS, and CUBIC for bone (Hama et al. 2015; Ke et al. 2016; Tainaka et al. 2018). Hydrogel-based methods include CLARITY and Bone CLARITY (Chung et al. 2013; Greenbaum et al. 2017). Gradient tB represents 30%, 50%, 70% *tert*-butanol solutions in the delipidation stage and 80%, 96%, 100% *tert*-butanol in the dehydration stage. Gradient THF includes various concentrations of tetrahydrofuran solutions; permeabilization solution contains Triton X-100, methyl-β-cyclodextrin, and trans-1-acetyl-4- hydroxy-L-proline; Sca*l*eS0 is a mixture of D-(–)-sorbitol, glycerol, methyl-β-cyclodextrin, γ-cyclodextrin, N-acetyl-L-hydroxyproline, and dimethylsulfoxide; Sca*l*eS1, Sca*l*eS2, Sca*l*eS3, and Sca*l*eS4 are mixtures of D-(–)-sorbitol, glycerol, urea, Triton X-100, and dimethylsulfoxide at different concentrations; CUBIC-L contains *N*-butyldiethanolamine and Triton X-100; CUBIC-B contains EDTA and imidazole; CUBIC-R/RA, 1:1 CUBIC-R/CUBIC-RA, and CUBIC-R contain antipyrine and nicotinamide; and CUBIC-RA contains antipyrine and *N*-methylnicotinamide. BABB, benzyl alcohol + benzyl benzoate; BABB-D, BABB + diphenyl ether (DPE); BBP, BB + modified poly(ethylene glycol); CUBIC-1, a mixture of urea, Quadrol, and Triton X-100; DCM, dichloromethane; EDTA, ethylenediaminetetraacetic acid; ETC, electrophoretic tissue clearing; Quadrol, (N,N,N′,N′-tetrakis(2-hydroxypropyl) ethylenediamine); PFA, paraformaldehyde; RIMS, refractive index matching solution with Histodenz as the main component; SDS, sodium dodecyl sulfate; tB-PEG, *tert*-butanol + modified poly(ethylene glycol).

solvent with a relatively high RI (RI >1.54). These methods have strong clearing capacity and high transparency. However, dehydration treatment is required for them, which causes tissue shrinkage and diminished or compromised endogenous green fluorescent protein (GFP) fluorescence.

2. Aqueous reagent-based TC techniques, including Sca*l*e (Hama et al. 2011; Hama et al. 2015), ClearT (Kuwajima et al. 2013), SeeDB series (Ke et al. 2013; Ke et al. 2016), CUBIC series (Tainaka et al. 2014; Kubota et al. 2017; Tainaka et al. 2018), Ce3D (Li et al. 2017), TDE (Costantini et al. 2015), FRUIT (Hou et al. 2015), sucrose (Tsai et al. 2009), and so on. Tissues are cleared through a series of aqueous solutions and finally RI matching is performed with aqueous clearing medium with a relatively low RI (RI 1.4 to 1.51). Most aqueous clearing methods preserve GFP fluorescence better than solvent-based methods, but the clearing outcome is usually less transparent.

3. Hydrogel-based TC techniques, including CLARITY (Chung and Deisseroth 2013), PACT (Treweek et al.

2015), and various modified protocols (Kim et al. 2015; Lee et al. 2016; Jensen and Berg 2017; Carrillo et al. 2018). These methods have unique procedures of hydrogel embedding for protecting protein components from harsh chemical or electrical treatments. These methods are mostly complicated and expensive.

In the current review, we will introduce general principles of clearing methods designed for clearing hard tissues and briefly describe commonly used clearing methods for bones and teeth. We will also provide basic background knowledge on 3-D imaging and data processing. Finally, we will introduce applications of tissue clearing on bone, dental, and neuroscience research.

General Principles for Clearing Hard Tissues

Components of hard tissues, including bones and teeth, are distinct from soft tissue organs: high mineralization, enriched collagen content, relatively low lipid content, and bone marrow space containing highly colorized blood cells. Such difference
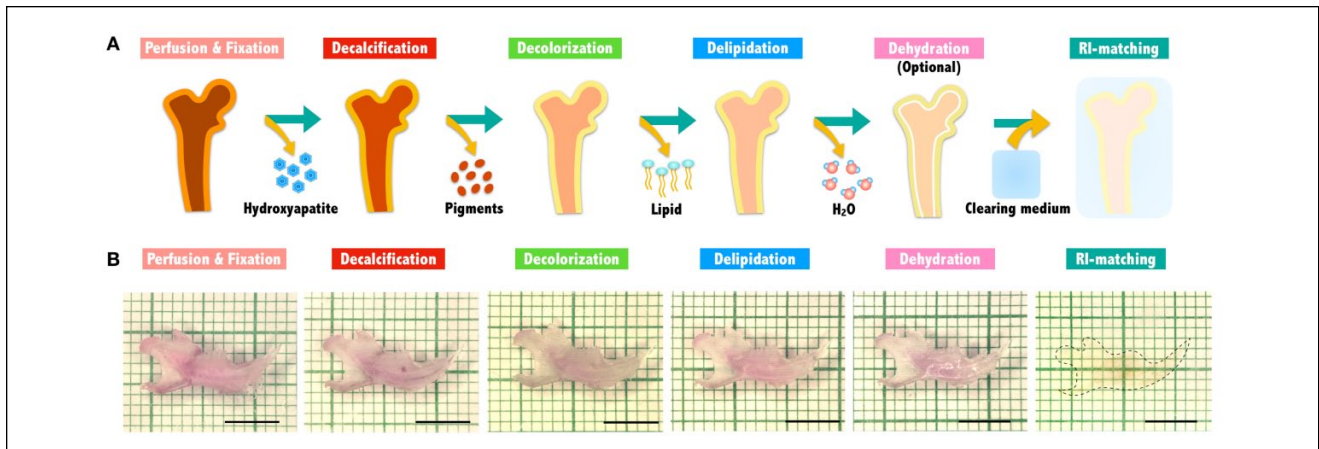
Figure 2. General principles for clearing hard tissues. (**A**) Similar treatment steps have been adapted by most tissue-clearing methods. (**B**) An adult mouse mandible was cleared following the PEGASOS method and images were taken after each treatment step. Dotted line outlines the nearly invisible mandible in the BB-PEG clearing medium. Scale bars, 5 mm. RI, refractive index.

constitutes a major challenge in applications of many tissue-clearing methods, which were mostly designed for clearing soft tissue organs. Therefore, some new methods were developed for hard tissue organs. Despite having different names and chemicals, all these methods follow similar principles to turn hard tissue transparent. Following are treatment steps used by most of the clearing methods for hard tissue organs (Fig. 2A).

Perfusion and Fixation

Transcardiac perfusion is the first step of all clearing methods. Immediately after general anesthesia, phosphate-buffered saline (PBS) or saline water is injected into the left ventricle to flush out the blood. Successful perfusion is indicated by liver lobes changing color from red to pale white. Complete perfusion is essential for removing blood from organs. Four percent paraformaldehyde (PFA) is the most commonly used fixative. Although PFA treatment significantly reduces endogenous GFP intensity, fixation helps GFP protein to resist harsh chemical treatments. Overlong PFA treatment does not provide extra protection benefit but denatures GFP protein permanently (Tainaka et al. 2016).

Decalcification

Both bones and teeth are enriched with calcium hydroxyapatite, which strongly blocks and diffracts light and makes hard tissue opaque (Bres et al. 1985; Simmons et al. 2011). Condensed crystal structure also prevents clearing medium from penetrating into deep regions. Therefore, decalcification is a critical step to achieve complete transparency. EDTA is the most commonly used decalcification reagent by many clearing methods. Its moderate decalcification efficacy protects tissue organization, antigen activity, and also endogenous fluorescence signals. Usually, 10% to 20% of EDTA solution with a pH of 7 to 8 has been used in various clearing methods

(Greenbaum et al. 2017; Savi et al. 2017; Jing et al. 2018). In the CUBIC method, EDTA was used in combination with *N*-butyldiethanolamine or imidazole to achieve better decalcification efficiency (Tainaka et al. 2018).

Decolorization

Endogenous pigments, most notably heme, in the bone marrow or dental pulp cavity interfere with light penetration and reduce imaging quality significantly. Hydrogen peroxide (H_2O_2) was the first decolorization reagent used by the iDISCO method (Renier et al. 2014). Its oxidative capacity rapidly bleaches nearly all pigment components, including heme, lipofuscin, and even melanin. Hydrogen peroxide treatment enhances both transparency and whole-mount immunostaining efficiency but also quenches all endogenous fluorescent signals (Alnuami et al. 2008; Renier et al. 2014). Quadrol (*N,N,N',N'*-tetrakis(2-hydroxypropyl) ethylenediamine) and *N*-butyldiethanolamine were developed by the CUBIC method. They were able to decolorize heme efficiently without compromising endogenous GFP signals. Quadrol functions possibly by binding to heme porphyrin and facilitating heme release under alkaline (pH 9–11) conditions (Tainaka et al. 2014; Tainaka et al. 2016). Later, Quadrol decolorization turned out to be highly effective and was also adapted by other clearing methods, including Bone CLARITY, PEGASOS, and vDISCO (Greenbaum et al. 2017; Jing et al. 2018; Cai et al. 2019).

Delipidation

Although less than 3% of the total bone matrix is lipid (Boskey 2013), delipidation treatment is still necessary to achieve final transparency. Various delipidation reagents have been used. Detergent, including sodium dodecyl sulfate (SDS), Triton X-100, thioglycerol, or saponin, has been used by aqueous clearing methods (Tomer et al. 2014; Ke et al. 2016; Li et al.

2017). Gradually increased solvent solutions, including ethanol, tetrahydrofuran (THF), and *tert*-butanol, have been used by solvent-based clearing methods. Overlong delipidation treatment with some reagents, including SDS and ethanol, can denature protein components and significantly compromise the endogenous GFP fluorescence (Becker et al. 2012; Treweek et al. 2015).

Dehydration for Solvent-Based Clearing Methods

Dehydration treatment is exclusively used by solvent-based clearing methods because the solvent-based clearing mediums are not miscible with water. Commonly used dehydration mediums include 100% ethanol, THF, *tert*-butanol, and tB-PEG (*tert*-butanol plus polyethylene glycol) (Erturk et al. 2012; Pan et al. 2016; Jing et al. 2018). Complete removal of water from the tissue causes tissue shrinkage and protein denature, which is likely a major cause of GFP fluorescence loss after clearing. In the PEGASOS method, a modified poly(ethylene glycol) (PEG) component within the tB-PEG dehydration medium was proposed to provide a relative friendly environment surrounding the GFP molecule and protect it from quenching (Jing et al. 2018).

RI Matching with Clearing Mediums

RI matching is the final step for all clearing treatments. Tissues are filled with homogeneous clearing solutions to achieve consistent internal RI and transparency. Generally, higher RI yields better transparency (Berke et al. 2016; Orlich and Kiefer 2017). Solvent-based clearing medium possesses higher RI (>1.54) than aqueous or hydrogel clearing mediums (RI 1.40 to 1.51). Most aqueous-based clearing methods are not efficient at clearing bones (Calve et al. 2015; Neu et al. 2015; Bykov et al. 2016). Hard tissues have a much higher intrinsic RI with the presence of calcium hydroxyapatite (RI ~1.63 to 1.65) and type I collagen (RI ~1.43). In contrast, RI of soft tissues, such as interstitial and intracellular fluid, is much lower (~1.35 to 1.37) (Ascenzi and Fabry 1959; Genina et al. 2008; Zhang et al. 2015). RI of type I collagen increases to 1.53 after dehydration (Wang et al. 1996). After decalcification, RI of bone is around 1.53 (Ascenzi and Fabry 1959). Therefore, solvent-based clearing methods produce better transparency than aqueous methods in clearing hard tissue samples. However, the absence of water within the solvent clearing medium makes them less amenable in preserving endogenous GFP activities (Tainaka et al. 2016).

TC Techniques for Clearing Hard Tissues

Modified Murray's Clear

Modified Murray's clearing method was the first approach for clearing hard tissues (Acar et al. 2015). The delipidation and dehydration steps are performed using a gradient ethanol solution series. Immunofluorescent staining is performed to detect GFP. Bones have to be bisected in order for antibodies and clearing medium to penetrate. No decalcification or decolorization process is performed. The final clearing medium is BABB (1:2 benzyl alcohol/benzyl benzoate) (RI ~1.55). Lack of endogenous fluorescence preservation is the major drawback.

DISCO Series

Preserving endogenous GFP activity is a major technical goal for most clearing methods. The first solvent-based clearing method application capable of preserving endogenous GFP partially is the 3DISCO method. Instead of alcohol, THF is used for delipidation and dehydration. Dibenzyl ether (DBE) (RI 1.56) is used to replace BABB as the clearing medium. THF dehydration is shown to produce less background fluorescence than ethanol dehydration (Becker et al. 2012), but THF is highly flammable and tends to form explosive peroxide when stored in air (Erturk et al. 2012).

The uDISCO method was later developed based on 3DISCO. *Tert*-butanol is used as the delipidation and dehydration solvent. Diphenyl ether (DPE) (RI 1.579) mixed with BABB is used as the clearing medium, and vitamin E is added to scavenge peroxides and to preserve endogenous GFP (Pan et al. 2016).

iDISCO is another variation of the 3DISCO method. Hydrogen peroxide is used to decolorize endogenous pigments and whole-mount immunofluorescent staining is performed before clearing treatment with the 3DISCO method (Renier et al. 2014; Belle et al. 2017). Decalcification is not included in the iDISCO or uDISCO method.

vDISCO is the most recent variant based on the uDISCO method. Decolorization treatment with Quadrol and decalcification with EDTA solution are included. Whole-mount nanobody staining against GFP is performed to enhance endogenous fluorescence and to reduce background (Cai et al. 2019).

All DISCO methods have achieved high transparency. Shrinkage of soft tissue from dehydration is a major drawback. Despite improved GFP fluorescence preservation, endogenous GFP fluorescence damage is still significant (Jing et al. 2018).

Bone CLARITY

Bone CLARITY is a hydrogel-based TC method specifically for hard tissues (Greenbaum et al. 2017). Bones are decalcified with EDTA solution for 14 d and then embedded with acrylamide hydrogel, delipidated with SDS solution, decolorized with Quadrol, and finally RI matched with special RIMS series (RI ~1.38 to 1.47). Excellent transparency is achieved for mouse long bone with strong endogenous GFP fluorescence. A major drawback is that its clearing effects on soft tissue organs are relatively poor, which limits its applications on organs of complex tissue types (Jing et al. 2018).

CUBIC Series

CUBIC methods are aqueous based. Identification of Quadrol as a decolorization reagent was a major breakthrough. The first

version of the CUBIC method did not include decalcification treatment. Decolorization and delipidation steps are performed with Sca/eCUBIC-1 composed of urea, Quadrol, Triton X-100, and water, after which tissues are cleared with Sca/eCUBIC-2 (RI ~1.48) composed of urea, sucrose, triethanolamine, and water. Sca/eCUBIC-2 is unable to clear bones (Tainaka et al. 2014).

A modified CUBIC method was developed later. Decolorization and delipidation are performed using CUBIC-L composed of Triton X-100 and *N*-buthyldiethanolamine. RI matching is performed using CUBIC-R (RI ~1.52) composed of antipyrine, nicotinamide, and water (Kubota et al. 2017). Improved RI greatly increases transparency but still cannot clear bone efficiently (Jing et al. 2018).

In the latest version of CUBIC method (CUBIC-B), decalcification with EDTA solution is incorporated and much better transparency is achieved for bone samples (Tainaka et al. 2018). Overall, the CUBIC series achieves high transparency and preserves endogenous fluorescence.

A major drawback of CUBIC methods is that the water component may evaporate during the imaging, which may reduce tissue transparency and produce precipitation.

PEGASOS

PEGASOS is a solvent-based clearing method applicable for both soft and hard tissues. It achieves superior transparency and provides better GFP preservation capability. Decalcification treatment is performed with 20% EDTA solution. Decolorization is performed using 25% Quadrol solution. Delipidation is performed using gradient *tert*-butanol (tB) solutions. Dehydration is performed using tB-PEG solvent composed of *tert*-butanol and modified PEG. RI matching is performed using BB-PEG medium (RI 1.543) composed of benzyl benzoate and modified polyethylene glycol (Fig. 2B). High transparency is achieved for both soft and hard tissue organs. In addition, PEGASOS preserves endogenous GFP fluorescence better than other solvent-based clearing methods, probably due to the high pH value of the solvent system and presence of modified PEG components (Jing et al. 2018). The major technical drawback is the shrinkage of soft tissue organs caused by dehydration. In addition, muscle tissue presents high autofluorescence after clearing (Jing et al. 2018).

3-D Imaging Acquisition for Cleared Hard Tissues

Cleared samples are usually kept within the clearing mediums for preservation and imaging. Three-dimensional deep imaging is different from conventional 2-dimensional (2-D) imaging. High resolution is required not only on the X-Y dimension (lateral resolution) but also on the vertical dimension (axial resolution). For a confocal or 2-photon microscope, lateral resolution $r_{xy} = k1 \times \lambda/NA$, and z-resolution $r_z = k2 \times n\lambda/NA^2$ (*k*1, *k*2, constants determined by the pinhole size; λ, wavelength of the illumination laser light; NA, numerical aperture).

Selection of proper objective is critical for a successful deep imaging. Noticeably, the resolution is determined mostly by the NA number but is irrelevant to the magnification. An objective with a higher NA number yields better lateral and axial resolutions. Working distance of the objective is another important parameter to consider. Sufficient working distance is essential for imaging through the full thickness of cleared samples.

Confocal Microscope

A confocal laser-scanning microscope (CLSM) uses a spatial pinhole to block any out-of-focus emission light signal to acquire high resolution. With high NA objective, the lateral resolution can easily reach 0.5 μm (NA >0.5). An objective of 0.5 NA can achieve an axial resolution of 5 to 10 μm. The major disadvantage of CLSM is the slow imaging speed. In our experience, ~8 h was needed on a CSLM to image a brain slice measuring $5 \times 8 \times 1$ mm with a 20× objective.

Resonant scanner is one approach to facilitate imaging speed and has been adapted by some latest CSLM models, including Leica SP8 and Nikon A1R. Imaging speed could be improved by 10- to 50-fold at the cost of increased background noise. Zeiss CSLM adapted a different strategy, named Airyscan (AS), to speed up the scanning rate (Kolossov et al. 2017). Alternatively, ribbon scanning confocal microscopy was developed with ~10- to 100-fold faster speed (Watson et al. 2017).

Two-Photon Microscope

A 2-photon microscope (2-P) relies on a nonlinear excitation reaction via a 2-photon excitation process (Nemoto et al. 2015). Some advantages include increased penetration depth, lower laser toxicity, and compatibility with a second harmonic generation (SHG) signal. SHG is a nonlinear optical effect in which second harmonic photons are generated by collagen and are half the wavelength of the excitation light (Vesuna et al. 2011; Acar et al. 2015). Such property is used for visualizing collagen-enriched bone or tooth structures (Fig. 3A, A′, A″). SHG signal can be detected in parallel with other fluorescence signals. It also possesses higher resolution (lateral resolution ~0.2 μm with a 1.0 NA objective) than that of any micro–computed tomography (μCT) (>0.5 μm). However, the 2-P microscope achieves lower lateral and axial resolution compared with a confocal microscope due to the much longer excitation wavelength (Doi et al. 2018). In addition, imaging speed of a 2-P microscope is slow due to its point-by-point scanning mode.

Light-Sheet Fluorescent Microscopy

Light-sheet fluorescent microscopy (LSFM) is the current trend for imaging large cleared samples. In contrast to CSLM, a thin slice of the sample is illuminated with a laser light sheet in the direction perpendicular to the imaging objective. LSFM significantly reduces the phototoxicity and background noise.
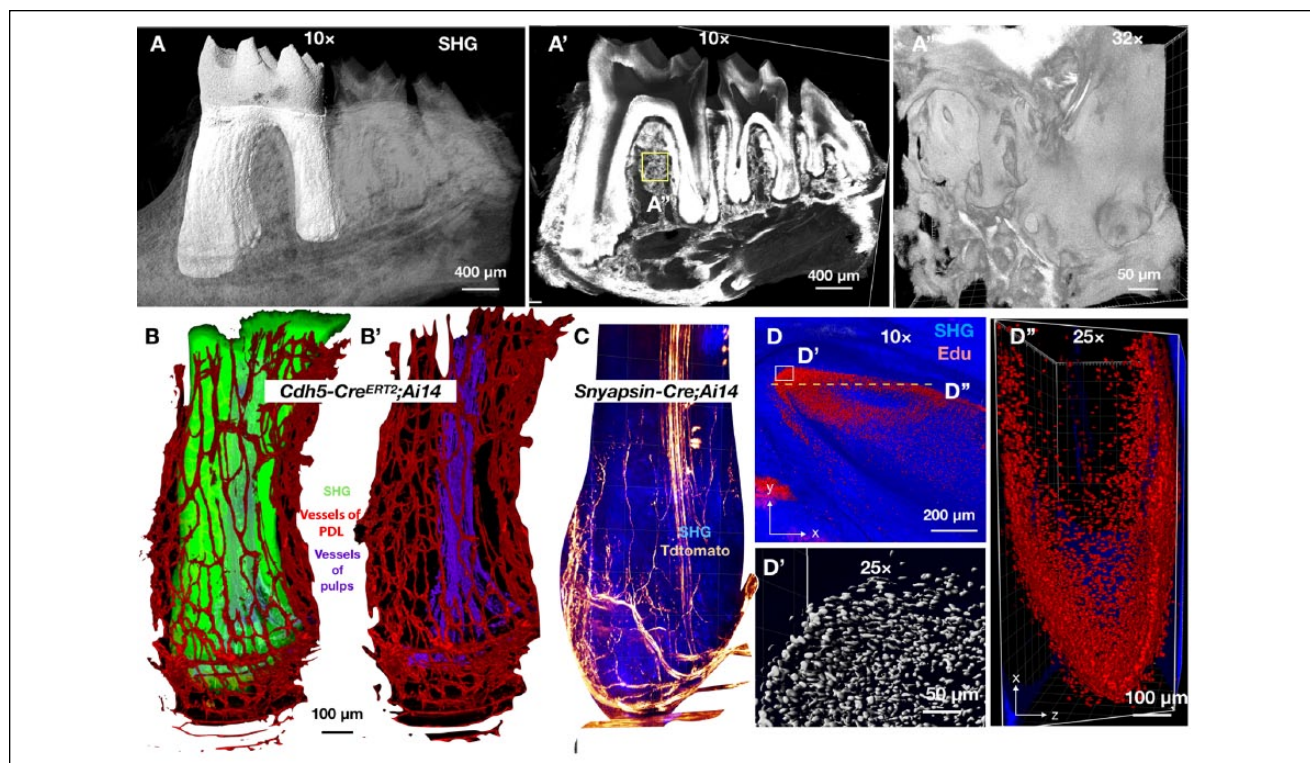
Figure 3. Application of PEGASOS clearing method for dental tissues. (**A**, **A′**, **A″**) An adult mouse mandible was cleared with the PEGASOS method (Jing et al. 2018). Second harmonic generation (SHG) signal was acquired with a 2-photon microscope. (A) The lower first molar is outlined within the mandible. (A′) Optical section shows the inside organization of the mandible. (A″) Boxed area in A′ was reimaged with a 32× objective to display the alveolar trabecular bone details. *Cdh5-Cre^{ERT2};Ai14* mice were induced with tamoxifen and sacrificed 7 d later. Mandible samples were cleared and imaged. (**B**) Mesial root of the lower first molar was imaged with a 2-photon microscope to display the blood vessels within the periodontal ligament (PDL) space; the cementum and dentin labeled by SHG were hidden to show the vasculatures of pulp and PDL converging at the apical region (**B′**). (**C**) *Synapsin-Cre;Ai14* mouse mandibles were cleared with the PEGASOS method and imaged with a 2-photon microscope to reveal nerve fibers within the PDL space of the lower first molar root. EdU was injected into mice 2 h before sacrifice. Mandible was processed for whole-mount EdU staining and clearing (Jing et al. 2018). (**D**) Edu labeled highly proliferative cells organized into a ring-like structure in the cervical loop region of the mouse incisor. (**D′**) Boxed region in E was enlarged and analyzed with Imaris 9.0 for 3-dimensional quantification. (**D″**) An X-Z optical section was acquired to display EdU+ cells' distribution pattern from a different perspective. Dotted line in (D) indicates position of the optical section.

Lateral resolution of LSFM is determined by the same formula as CSLM. The axial resolution is mainly determined by the dimension of the thinnest part of the light sheet (beam waist). LSFM scans samples using a plane of light instead of a point. Therefore, the image acquisition speeds can be 100 to 1,000 times faster than that of CLSM or a 2-P microscope. Applications of LSFM have been demonstrated by many TC studies, including CLARITY, CUBIC, uDISCO, SeeDB2, and Bone CLARITY (Susaki et al. 2014; Ke et al. 2016; Pan et al. 2016; Greenbaum et al. 2017). Some LSFM has become commercially available in recent years, such as Ultra Microscope II (La Vision), Zeiss Z1, and a tiling light-sheet microscope (Intelligent Imaging Innovations 3I) (Fu et al. 2016). Insufficient resolution is the major drawback of the LSFM.

Data Processing for 3-D Images of Cleared Tissues

Imaging of large cleared samples easily generates a large data set of 1 GB to 1 TB in size depending on the sample size, resolution, and color depth. A high-performance workstation is required for data storage and processing. We recommend an optimal system configuration as follows: 128 GB RAM, dual CPU, high-end graphic card (Nvidia GTX 1080 Ti or AMD Radeon 580), and large storage hard drives (>5 TB).

ImageJ (National Institutes of Health)

ImageJ is an open-source freeware that is commonly used by most 3-D imaging projects (Schindelin et al. 2012). It provides most routine image-processing functions, including format conversion, imaging stack and channel operation, image adjustment, and image quantification. Its functions are further expanded by updates and plug-ins written by other users. A current version of ImageJ has crashed frequently on handling large data sets.

Imaris (Bitplane)

Imaris is a popular commercial 3-D visualization and analysis software package. It provides function modules, including 3-D rendering, video making, image segmentation, and neuron
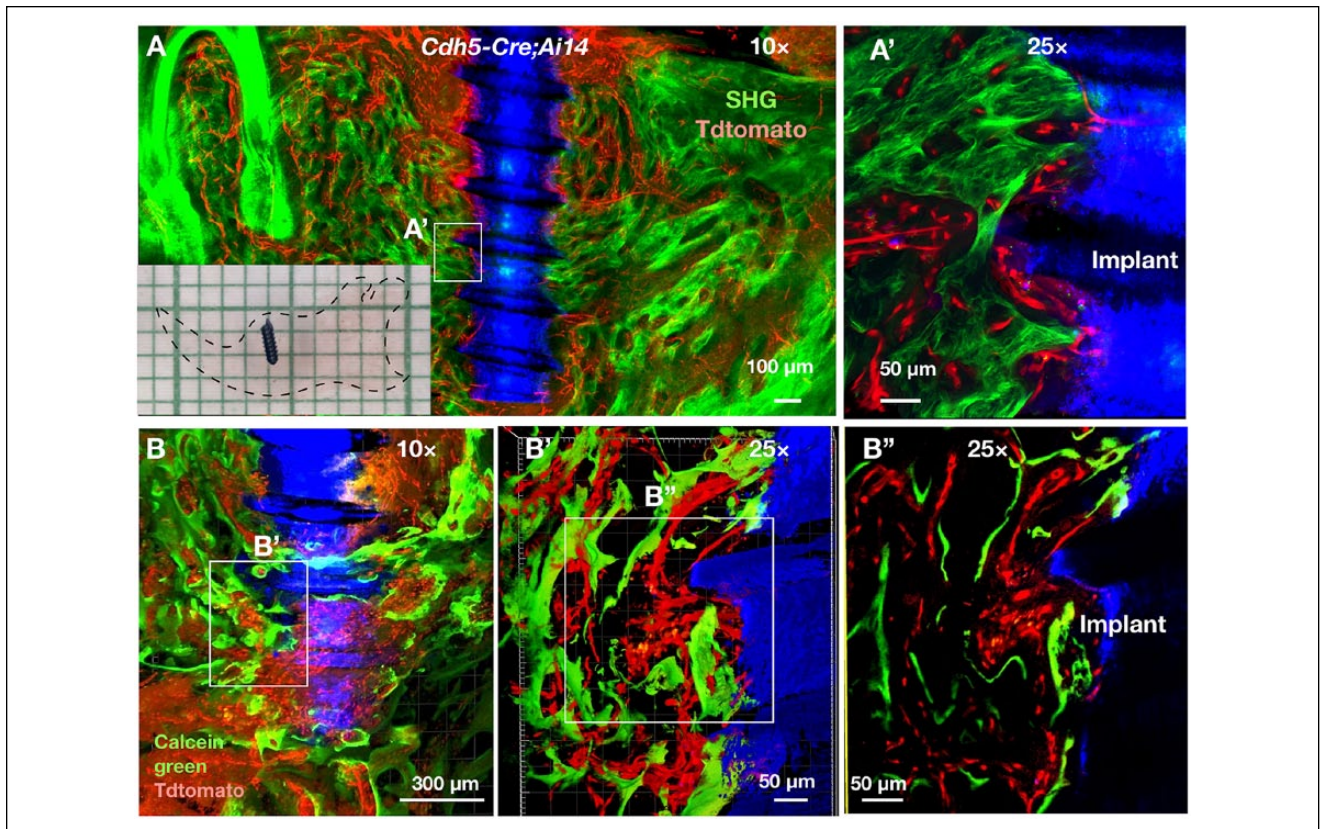
Figure 4. The 3-dimensional visualization of implant-tissue interface with the PEGASOS clearing method. *Cdh5-Cre^ERT2;Ai14* mice were induced with tamoxifen to label the vasculature endothelium. The lower first molar was extracted and a titanium implant was placed immediately. Calcein green was injected 2 h prior to sacrifice. Samples were collected 1 mo later and cleared with the PEGASOS method with (**A**) or without (**B**) decalcification treatment. (A) Cleared mandible was imaged with a 2-photon microscope showing blood vessels at the intact implant-bone interface. Implant was revealed with the reflection image (blue). Blood vessels were shown with tdTomato signal (red). Bone as shown with the second harmonic generation (SHG) signal (green). Inset shows a cleared mandible sample with the titanium implant. (**A′**) Boxed area in (A) was reimaged with a 25× objective to display direct contacts among blood vessels, bone, and implant surface. (B) Calcein green signal (green) indicates active bone remodeling activity near the implant surface. (**B′**) Boxed area in (B) was enlarged to show blood vessels (red) and calcein green signal (green) in direct contact with the implant surface (blue). (**B″**) An optical section was acquired to show the spatial relationship among implant surface, vasculatures, and calcein green signal.

tracing. The processing speed is also faster due to optimized hardware support. It is more user-friendly than ImageJ but is expensive ($10,000 to $70,000) for individual labs.

Applications of Tissue Clearing on Bone, Oral, and Neural Tissues

In recent years, TC techniques have found their applications on hard tissue research. Here we summarize their applications on bone research, dental research, and neuroscience research related to hard tissues.

Application of TC in Bone Research

Bone marrow is a highly complicated environment containing hematopoietic stem cells (HSCs), mesenchymal stem cells (MSCs), nerves, and various types of vasculatures organized in complicated spatial patterns. Conventional 2-D sections provide limited information. With bisected mouse long bone

samples, multiplex immunofluorescent staining is performed, including c-kit and α-catulin-GFP for HSCs, laminin for vasculature endothelium, and SHG for bone. Three-dimensional images reveal a close association of HSC populations with vasculature endothelium (Acar et al. 2015). In another study, bone marrow plug was removed from the marrow space for immunofluorescent staining and cleared with the CUBIC method. The 3-D images revealed that >94% of Hoxb5+ HSCs are directly attached to the abluminal surface of VE-cadherin+ endothelial cells. Both results demonstrated that long-term HSCs are not evenly distributed within the bone marrow (Chen et al. 2016). Vasculature within bone marrow also has been investigated by using other TC techniques combined with various antibodies or transgenic models, including anti-CD31 antibody (Woo et al. 2016; Klingberg et al. 2017), dextran dye (Pan et al. 2016), α*SMA-Cre^ERT;Ai14* mice, *Tie2-Cre;Ai14* mice (Jing et al. 2018) and *Cdh5-Cre^ERT2;Ai14* mice (Yi et al. 2019), *actin-DsRed* reporter mice (Li et al. 2017), and *mT/mG* transgenic mice (Calve et al. 2015). Recently, the lymphatic connections between calvaria bone and meninges were investigated using
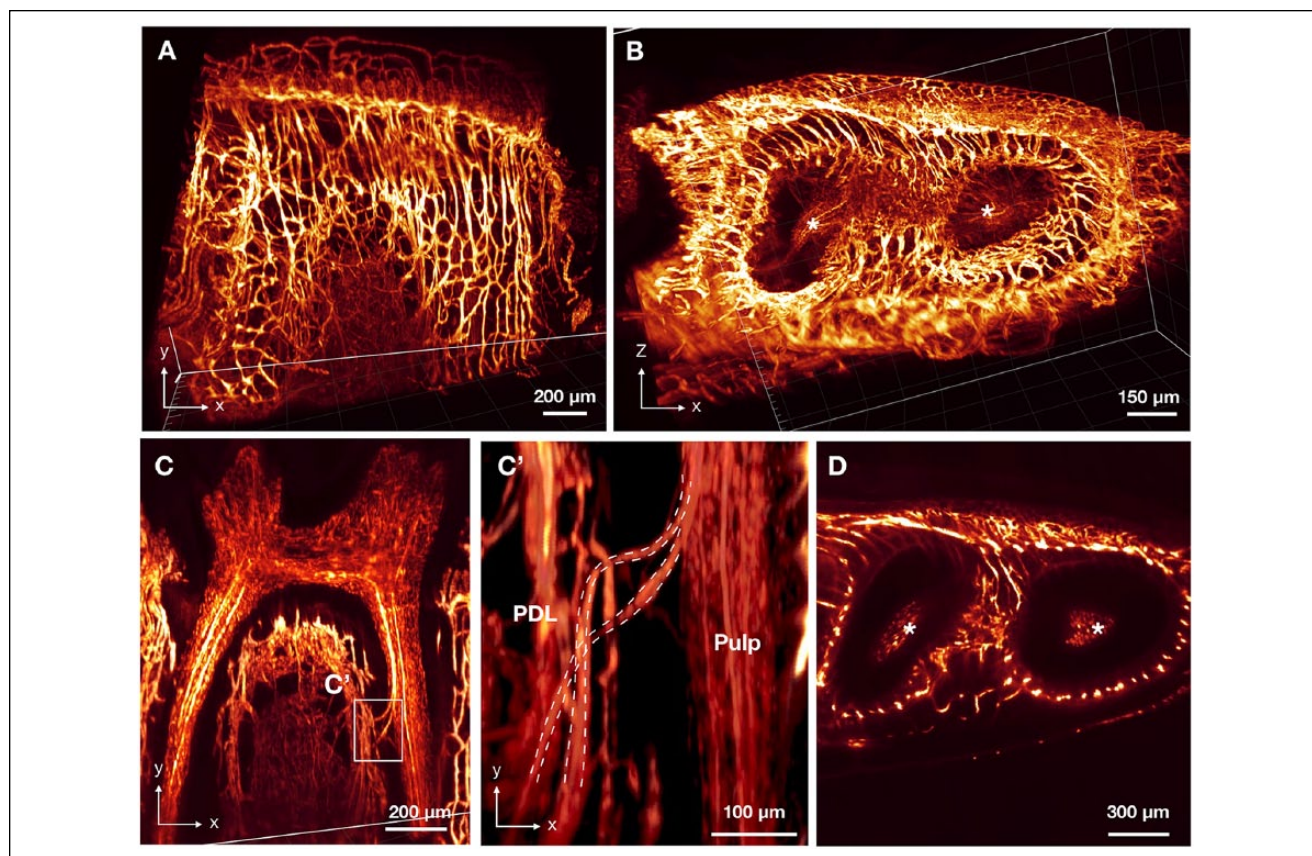
Figure 5. High-speed acquisition of vasculature within and surrounding the mouse molar with a tiling light-sheet microscope. *Cdh5-Cre^{ERT2};Ai14* mice were induced with tamoxifen to label the vascular endothelium. Mandibles were collected 1 wk later and cleared following a slightly modified PEGASOS protocol. The first molar area was imaged with a tiling light-sheet microscope provided by the Intelligent Imaging Innovations (3I) (Fu et al. 2016). Image stack is displayed in X-Y (**A**) and Y-Z (**B**) directions, respectively. Asterisks indicate the pulp vasculature. (**C**) An optical slice was acquired on the X-Y direction to display the pulp vasculature. (**C′**) Boxed region in C was enlarged to show communication vessels between the pulp and periodontal ligament (PDL). (**D**) A horizontal optical section was acquired. Asterisks indicate pulp vasculature.

the vDISCO method. Whole-head imaging revealed lymphatic vessels located between brain and skull bones (Cai et al. 2019).

Bone marrow was also the niche for MSCs. Based on the Bone CLARITY method, *Sox9*+ progenitor cells within mouse long bone were investigated. The 3-D images showed distinct *Sox9*+ stem cell quantities between healthy and diseased conditions (Greenbaum et al. 2017). Based on the uDISCO method based on whole-body imaging, distribution of transplanted bone marrow MSCs in the recipient mice showed that most of the transplanted BMSCs were trapped within the lungs (Pan et al. 2016; Guo et al. 2017).

Application of TC in Dental Research

The TC technique found the first application in dental tissue research with the PEGASOS method due to its strong clearing and GFP preservation capabilities. Based on transgenic mouse models including *Tie2-Cre;Ai14* mice or *Cdh5-Cre^{ERT2};Ai14* mice, the PEGASOS clearing method enabled visualization of blood vessels within the pulp chamber and the periodontal ligament (PDL) space in 3 dimensions (Jing et al. 2018) (Fig. 3B, B′). Based on *Synapsin-Cre;Ai14* mice, the nerve network

within the PDL space and pulp chamber was visualized in 3-D (Fig. 3C). Mouse incisor is known to contain highly proliferative transit-amplifying (TA) cells near the cervical loop. Based on EdU incorporation labeling and the PEGASOS method, TA cells within a mouse incisor were visualized and quantified in 3 dimensions (Fig. 3D, D′, D″). Treatment with cytosine arabinoside, a chemotherapy drug, significantly reduced TA cell numbers (Jing et al. 2018).

The PEGASOS clearing method was also applied for bone-implant interface research. The PEGASOS clearing method efficiently rendered decalcified or nondecalcified mandible bones transparent while preserving endogenous GFP signal (Fig. 4A, inset). The implant-bone interface could be directly imaged under a confocal or 2-P microscope (Fig. 4A, A′). Multichannel 3-dimensional images of the bone-implant interface were acquired (Fig. 4). The image depth could reach >800 μm with a decalcified mandible sample or ~400 μm for nondecalcified samples. Osteogenesis and angiogenesis processes after implant placement were investigated (Yi et al. 2019). Clearing of nondecalcified mandible samples enabled visualization of calcein green labeling signal (Fig. 4B, B′, B″).
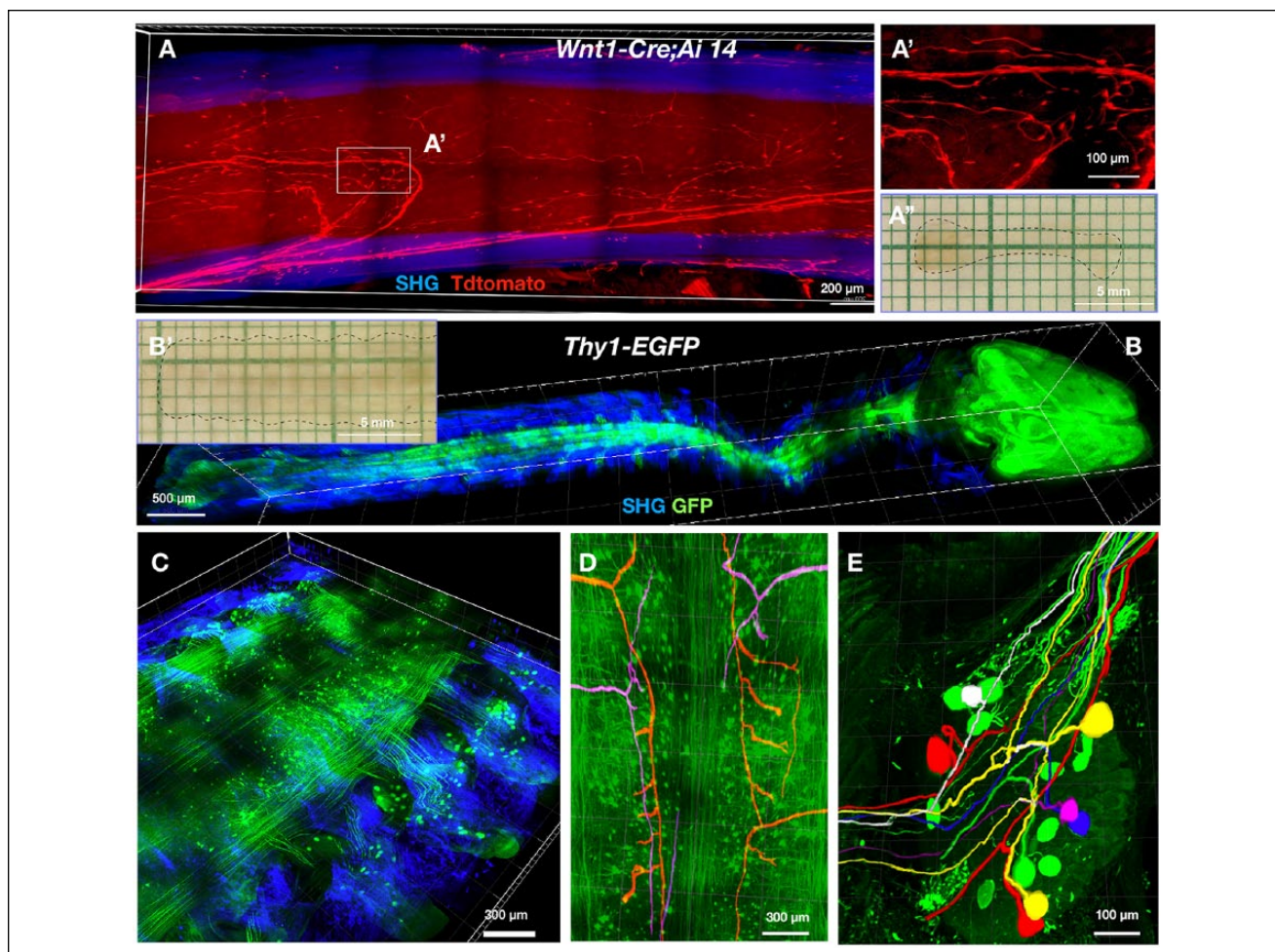
Figure 6. The 3-dimensional images of neural tissues within bones. Tibia bones were harvested from adult *Wnt1-Cre;Ai14* mice. Vertebrae were collected from adult *Thy1-EGFP* mice. Samples were cleared following the PEGASOS method (Jing et al. 2018). Cleared samples were imaged with a 2-photon or confocal microscope. (**A**) Nerve fibers (tdTomato signal) within the tibia (second harmonic generation [SHG] signal) bone marrow space. (**A′**) Boxed region in (A) was enlarged to show nerves and associated Schwann cells. (**A″**) Cleared tibia bone was imaged with a stereomicroscope. Dotted line outlines the form. (**B**) The entire central nervous system, including the brain and spinal cord, was imaged with a 5× objective without removing the vertebrae bone. (**B′**) A segment of vertebrae after clearing was imaged with a stereomicroscope. Dotted line outlines its form. (**C**) A segment of cervical vertebrae was imaged with a 10× objective to show spinal cord (green signal) within the vertebrae bone (SHG signal). (**D**) A segment of cervical spinal cord was imaged with a 10× objective on a confocal microscope. Individual axons together with their side branches were artificially labeled with different colors. (**E**) A dorsal root ganglion (DRG) was imaged through the vertebrae with a 20× objective on a confocal microscope to reveal individual DRG neurons together with their central or peripheral axons. Each neuron was artificially labeled with different colors.

Based on *Cdh5-Cre^{ERT2};Ai14* mice, we also used a tiling light-sheet microscope (Fu et al. 2016) (3I, Inc.) to image blood vessels surrounding and inside the molar. Complete vascular network was visualized with comparable quality as with a confocal microscope but within a much shorter time (<0.5 h vs. 5 h with a confocal microscope) (Fig. 5A–D).

Application of TC in Neuroscience Research Related to Hard Tissues

Within the bone marrow, neural regulation was proposed to be a critical niche factor for HSCs (Hanoun et al. 2015). Based on the *Wnt1-Cre;Ai14* mouse model for labeling peripheral nerves and the PEGASOS clearing method, nerves within bone

marrow space were revealed. The 3-D imaging indicated that nerves and arteries presented distinct distribution densities within the bone marrow space (Fig. 6A, A′, A″). Dorsal root ganglions (DRGs) are the relay ganglions between the central and peripheral nervous systems, which are difficult to be separated from surrounding bone structures (Malin et al. 2007). Based on the *Thy1-EGFP* mouse model for labeling nerves and PEGASOS clearing method, the 3-D images of the entire spinal cord were acquired without isolating it from the vertebrae. Individual DRG neurons and their peripheral and central axon branches were clearly identified and traced (Fig. 6B–E) (Jing et al. 2018). Recently, the vDISCO clearing method was applied for *Thy1-GFP* mice to investigate the innervation within muscles of vertebra and lower limbs. Nanobody

staining was used for enhancing endogenous GFP signals and reducing background fluorescence. The 3-D morphological changes of peripheral nerve terminals upon traumatic brain injury were revealed (Cai et al. 2019).

Conclusions and Perspective

No individual clearing method is perfect for all applications. Depending on research purposes, the following are 3 criteria for selecting appropriate methods: transparency outcome, fluorescent preservation, and tissue applicability.

The TC technique is still facing many challenges. Whole-mount immunohistochemical staining is one of them. Penetration of antibodies into deep regions is extremely challenging due to the large molecular weight (~150 kDa for IgG antibody) (Brinkmann and Kontermann 2017). Immunohistochemical staining of large bone tissue remains nearly impossible even with decalcification. Nanobody is a promising solution, which is produced from camel or fish and is only one-tenth of regular antibodies. It provides much better tissue penetrance (Fridy et al. 2014). Another technical challenge is the slow acquisition speed of conventional microscopic systems. Light-sheet microscopic systems are promising solutions but still need further improvement on their resolution.

Author Contributions

D. Jing, H. Zhao, contributed to conception, design, data acquisition, analysis, and interpretation, drafted and critically revised the manuscript; Y. Yi, W. Luo, S. Zhang, E. Lachika, contributed to data acquisition, critically revised the manuscript; Q. Yuan, J. Wang, contributed to data interpretation, critically revised the manuscript; Z. Zhao, contributed to design and data analysis, drafted and critically revised the manuscript. All authors gave final approval and agree to be accountable for all aspects of the work.

Acknowledgments

References

Acar M, Kocherlakota KS, Murphy MM, Peyer JG, Oguro H, Inra CN, Jaiyeola C, Zhao Z, Luby-Phelps K, Morrison SJ. 2015. Deep imaging of bone marrow shows non-dividing stem cells are mainly perisinusoidal. Nature. 526(7571):126–130.

Alnuami AA, Zeedi B, Qadri SM, Ashraf SS. 2008. Oxyradical-induced GFP damage and loss of fluorescence. Int J Biol Macromol. 43(2):182–186.

Ascenzi A, Fabry C. 1959. Technique for dissection and measurement of refractive index of osteones. J Biophys Biochem Cytol. 6(1):139–142.

Becker K, Jahrling N, Saghafi S, Weiler R, Dodt HU. 2012. Chemical clearing and dehydration of gfp expressing mouse brains. PLoS One. 7(3):e33916.

Belle M, Godefroy D, Couly G, Malone SA, Collier F, Giacobini P, Chedotal A. 2017. Tridimensional visualization and analysis of early human development. Cell. 169(1):161–173.e112.

Berke IM, Miola JP, David MA, Smith MK, Price C. 2016. Seeing through musculoskeletal tissues: improving in situ imaging of bone and the lacunar canalicular system through optical clearing. PLoS One. 11(3):e0150268.

Boskey AL. 2013. Bone composition: relationship to bone fragility and anti-osteoporotic drug effects. Bonekey Rep. 2:447. Erratum in: Bonekey Rep. 2015;4:710.

Bres EF, Barry JC, Hutchison JL. 1985. High-resolution electron microscope and computed images of human tooth enamel crystals. J Ultrastruct Res. 90(3):261–274.

Brinkmann U, Kontermann RE. 2017. The making of bispecific antibodies. MAbs. 9(2):182–212.

Bykov A, Hautala T, Kinnunen M, Popov V, Karhula S, Saarakkala S, Nieminen MT, Tuchin V, Meglinski I. 2016. Imaging of subchondral bone by optical coherence tomography upon optical clearing of articular cartilage. J Biophotonics. 9(3):270–275.

Cai R, Pan C, Ghasemigharagoz A, Todorov MI, Forstera B, Zhao S, Bhatia HS, Parra-Damas A, Mrowka L, Theodorou D, et al. 2019. Panoptic imaging of transparent mice reveals whole-body neuronal projections and skull-meninges connections. Nat Neurosci. 22(2):317–327.

Calve S, Ready A, Huppenbauer C, Main R, Neu CP. 2015. Optical clearing in dense connective tissues to visualize cellular connectivity in situ. PLoS One. 10(1):e0116662.

Carrillo M, Chuecos M, Gandhi K, Bednov A, Moore DL, Maher J, Ventolini G, Ji G, Schlabritz-Loutsevitch N. 2018. Optical tissue clearing in combination with perfusion and immunofluorescence for placental vascular imaging. Medicine (Baltimore). 97(39):e12392.

Chen JY, Miyanishi M, Wang SK, Yamazaki S, Sinha R, Kao KS, Seita J, Sahoo D, Nakauchi H, Weissman IL. 2016. Hoxb5 marks long-term haematopoietic stem cells and reveals a homogenous perivascular niche. Nature. 530(7589):223–227.

Chung K, Deisseroth K. 2013. Clarity for mapping the nervous system. Nat Methods. 10(6):508–513.

Chung K, Wallace J, Kim SY, Kalyanasundaram S, Andalman AS, Davidson TJ, Mirzabekov JJ, Zalocusky KA, Mattis J, Denisin AK, et al. 2013. Structural and molecular interrogation of intact biological systems. Nature. 497(7449):332–337.

Costantini I, Ghobril JP, Di Giovanna AP, Allegra Mascaro AL, Silvestri L, Mullenbroich MC, Onofri L, Conti V, Vanzi F, Sacconi L, et al. 2015. A versatile clearing agent for multi-modal brain imaging. Sci Rep. 5:9808.

Dodt HU, Leischner U, Schierloh A, Jahrling N, Mauch CP, Deininger K, Deussing JM, Eder M, Zieglgansberger W, Becker K. 2007. Ultramicroscopy: three-dimensional visualization of neuronal networks in the whole mouse brain. Nat Methods. 4(4):331–336.

Doi A, Oketani R, Nawa Y, Fujita K. 2018. High-resolution imaging in two-photon excitation microscopy using in situ estimations of the point spread function. Biomed Opt Express. 9(1):202–213.

Erturk A, Becker K, Jahrling N, Mauch CP, Hojer CD, Egen JG, Hellal F, Bradke F, Sheng M, Dodt HU. 2012. Three-dimensional imaging of solvent-cleared organs using 3disco. Nat Protoc. 7(11):1983–1995.

Fridy PC, Li Y, Keegan S, Thompson MK, Nudelman I, Scheid JF, Oeffinger M, Nussenzweig MC, Fenyo D, Chait BT, et al. 2014. A robust pipeline for rapid production of versatile nanobody repertoires. Nat Methods. 11(12):1253–1260.

Fu Q, Martin BL, Matus DQ, Gao L. 2016. Imaging multicellular specimens with real-time optimized tiling light-sheet selective plane illumination microscopy. Nat Commun. 7:11088.

Genina EA, Bashkatov AN, Tuchin VV. 2008. Optical clearing of cranial bone. Adv Optical Technol. 2008(267867):1–8.

Greenbaum A, Chan KY, Dobreva T, Brown D, Balani DH, Boyce R, Kronenberg HM, McBride HJ, Gradinaru V. 2017. Bone clarity: clearing, imaging, and computational analysis of osteoprogenitors within intact bone marrow. Sci Transl Med. 9(387). pii: eaah6518.

Guo W, Imai S, Yang JL, Zou S, Watanabe M, Chu YX, Mohammad Z, Xu H, Moudgil KD, Wei F, et al. 2017. In vivo immune interactions of multipotent stromal cells underlie their long-lasting pain-relieving effect. Sci Rep. 7(1):10107.

Hama H, Hioki H, Namiki K, Hoshida T, Kurokawa H, Ishidate F, Kaneko T, Akagi T, Saito T, Saido T, et al. 2015. Scales: an optical clearing palette for biological imaging. Nat Neurosci. 18(10):1518–1529.

Hama H, Kurokawa H, Kawano H, Ando R, Shimogori T, Noda H, Fukami K, Sakaue-Sawano A, Miyawaki A. 2011. Scale: a chemical approach for fluorescence imaging and reconstruction of transparent mouse brain. Nat Neurosci. 14(11):1481–1488.

Hanoun M, Maryanovich M, Arnal-Estape A, Frenette PS. 2015. Neural regulation of hematopoiesis, inflammation, and cancer. Neuron. 86(2):360–373.

Hou B, Zhang D, Zhao S, Wei M, Yang Z, Wang S, Wang J, Zhang X, Liu B, Fan L, et al. 2015. Scalable and DiI-compatible optical clearance of the mammalian brain. Front Neuroanat. 9:19.

Jensen KHR, Berg RW. 2017. Advances and perspectives in tissue clearing using clarity. J Chem Neuroanat. 86:19–34.

Jing D, Zhang S, Luo W, Gao X, Men Y, Ma C, Liu X, Yi Y, Bugde A, Zhou BO, et al. 2018. Tissue clearing of both hard and soft tissue organs with the PEGASOS method. Cell Res. 28(8):803–818.

Ke MT, Fujimoto S, Imai T. 2013. SeeDB: a simple and morphology-preserving optical clearing agent for neuronal circuit reconstruction. Nat Neurosci. 16(8):1154–1161.

Ke MT, Nakai Y, Fujimoto S, Takayama R, Yoshida S, Kitajima TS, Sato M, Imai T. 2016. Super-resolution mapping of neuronal circuitry with an index-optimized clearing agent. Cell Rep. 14(11):2718–2732.

Kim SY, Cho JH, Murray E, Bakh N, Choi H, Ohn K, Ruelas L, Hubbert A, McCue M, Vassallo SL, et al. 2015. Stochastic electrotransport selectively enhances the transport of highly electromobile molecules. Proc Natl Acad Sci U S A. 112(46):E6274–E6283.

Klingberg A, Hasenberg A, Ludwig-Portugall I, Medyukhina A, Mann L, Brenzel A, Engel DR, Figge MT, Kurts C, Gunzer M. 2017. Fully automated evaluation of total glomerular number and capillary tuft size in nephritic kidneys using lightsheet microscopy. J Am Soc Nephrol. 28(2):452–459.

Kolossov VL, Sivaguru M, Huff J, Luby K, Kanakaraju K, Gaskins HR. 2017. Airyscan super-resolution microscopy of mitochondrial morphology and dynamics in living tumor cells. Microsc Res Tech. 81(2):115–128.

Kubota SI, Takahashi K, Nishida J, Morishita Y, Ehata S, Tainaka K, Miyazono K, Ueda HR. 2017. Whole-body profiling of cancer metastasis with single-cell resolution. Cell Rep. 20(1):236–250.

Kuwajima T, Sitko AA, Bhansali P, Jurgens C, Guido W, Mason C. 2013. Cleart: A detergent- and solvent-free clearing method for neuronal and non-neuronal tissue. Development. 140(6):1364–1368.

Lee E, Choi J, Jo Y, Kim JY, Jang YJ, Lee HM, Kim SY, Lee HJ, Cho K, Jung N, et al. 2016. Act-presto: Rapid and consistent tissue clearing and labeling method for 3-dimensional (3D) imaging. Sci Rep. 6:18631.

Li W, Germain RN, Gerner MY. 2017. Multiplex, quantitative cellular analysis in large tissue volumes with clearing-enhanced 3d microscopy (CE3D). Proc Natl Acad Sci U S A. 114(35):E7321–E7330.

Malin SA, Davis BM, Molliver DC. 2007. Production of dissociated sensory neuron cultures and considerations for their use in studying neuronal function and plasticity. Nat Protoc. 2(1):152–160.

Nemoto T, Kawakami R, Hibi T, Iijima K, Otomo K. 2015. Two-photon excitation fluorescence microscopy and its application in functional connectomics. Microscopy (Oxf). 64(1):9–15.

Neu CP, Novak T, Gilliland KF, Marshall P, Calve S. 2015. Optical clearing in collagen- and proteoglycan-rich osteochondral tissues. Osteoarthritis Cartilage. 23(3):405–413.

Orlich M, Kiefer F. 2017. A qualitative comparison of ten tissue clearing techniques. Histol Histopathol. 33(2):181–199.

Pan C, Cai R, Quacquarelli FP, Ghasemigharagoz A, Lourbopoulos A, Matryba P, Plesnila N, Dichgans M, Hellal F, Erturk A. 2016. Shrinkage-mediated imaging of entire organs and organisms using uDISCO. Nat Methods. 13(10):859–867.

Renier N, Wu Z, Simon DJ, Yang J, Ariel P, Tessier-Lavigne M. 2014. IDISCO: a simple, rapid method to immunolabel large tissue samples for volume imaging. Cell. 159(4):896–910.

Savi FM, Brierly GI, Baldwin J, Theodoropoulos C, Woodruff MA. 2017. Comparison of different decalcification methods using rat mandibles as a model. J Histochem Cytochem. 65(12):705–722.

Schindelin J, Arganda-Carreras I, Frise E, Kaynig V, Longair M, Pietzsch T, Preibisch S, Rueden C, Saalfeld S, Schmid B, et al. 2012. Fiji: an open-source platform for biological-image analysis. Nat Methods. 9(7):676–682.

Schwarz MK, Scherbarth A, Sprengel R, Engelhardt J, Theer P, Giese G. 2015. Fluorescent-protein stabilization and high-resolution imaging of cleared, intact mouse brains. PLoS One. 10(5):e0124650.

Seo J, Choe M, Kim SY. 2016. Clearing and labeling techniques for large-scale biological tissues. Mol Cells. 39(6):439–446.

Simmons LM, Al-Jawad M, Kilcoyne SH, Wood DJ. 2011. Distribution of enamel crystallite orientation through an entire tooth crown studied using synchrotron X-ray diffraction. Eur J Oral Sci. 119(Suppl 1):19–24.

Spalteholz W. 1914. Uber das durchsichtigmachen von menschlichen und tierischen praparaten [About the transparency of human and animal preparations]. Hierzal, Leipzig.

Steinke H, Wolff W. 2001. A modified spalteholz technique with preservation of the histology. Ann Anat. 183(1):91–95.

Susaki EA, Tainaka K, Perrin D, Kishino F, Tawara T, Watanabe TM, Yokoyama C, Onoe H, Eguchi M, Yamaguchi S, et al. 2014. Whole-brain imaging with single-cell resolution using chemical cocktails and computational analysis. Cell. 157(3):726–739.

Susaki EA, Ueda HR. 2016. Whole-body and whole-organ clearing and imaging techniques with single-cell resolution: toward organism-level systems biology in mammals. Cell Chem Biol. 23(1):137–157.

Tainaka K, Kubota SI, Suyama TQ, Susaki EA, Perrin D, Ukai-Tadenuma M, Ukai H, Ueda HR. 2014. Whole-body imaging with single-cell resolution by tissue decolorization. Cell. 159(4):911–924.

Tainaka K, Kuno A, Kubota SI, Murakami T, Ueda HR. 2016. Chemical principles in tissue clearing and staining protocols for whole-body cell profiling. Annu Rev Cell Dev Biol. 32:713–741.

Tainaka K, Murakami TC, Susaki EA, Shimizu C, Saito R, Takahashi K, Hayashi-Takagi A, Sekiya H, Arima Y, Nojima S, et al. 2018. Chemical landscape for tissue clearing based on hydrophilic reagents. Cell Rep. 24(8):2196–2210.e2199.

Tomer R, Ye L, Hsueh B, Deisseroth K. 2014. Advanced clarity for rapid and high-resolution imaging of intact tissues. Nat Protoc. 9(7):1682–1697.

Treweek JB, Chan KY, Flytzanis NC, Yang B, Deverman BE, Greenbaum A, Lignell A, Xiao C, Cai L, Ladinsky MS, et al. 2015. Whole-body tissue stabilization and selective extractions via tissue-hydrogel hybrids for high-resolution intact circuit mapping and phenotyping. Nat Protoc. 10(11):1860–1896.

Tsai PS, Kaufhold JP, Blinder P, Friedman B, Drew PJ, Karten HJ, Lyden PD, Kleinfeld D. 2009. Correlations of neuronal and microvascular densities in murine cortex revealed by direct counting and colocalization of nuclei and vessels. J Neurosci. 29(46):14553–14570.

Vesuna S, Torres R, Levene MJ. 2011. Multiphoton fluorescence, second harmonic generation, and fluorescence lifetime imaging of whole cleared mouse organs. J Biomed Opt. 16(10):106009.

Wang XJ, Milner TE, Chang MC, Nelson JS. 1996. Group refractive index measurement of dry and hydrated type i collagen films using optical low-coherence reflectometry. J Biomed Opt. 1(2):212–216.

Watson AM, Rose AH, Gibson GA, Gardner CL, Sun C, Reed DS, Lam LKM, St Croix CM, Strick PL, Klimstra WB, et al. 2017. Ribbon scanning confocal for high-speed high-resolution volume imaging of brain. PLoS One. 12(7):e0180486.

Woo J, Lee M, Seo JM, Park HS, Cho YE. 2016. Optimization of the optical transparency of rodent tissues by modified pact-based passive clearing. Exp Mol Med. 48(12):e274.

Yi Y, Men Y, Jing D, Luo W, Zhang S, Feng JQ, Liu J, Ge WP, Wang J, Zhao H. 2019. 3-Dimensional visualization of implant-tissue interface with the polyethylene glycol associated solvent system tissue clearing method. Cell Prolif [epub ahead of print 3 Feb 2019]. DOI: 10.1111/cpr.12578

Zhang Y, Zhang C, Zhong X, Zhu D. 2015. Quantitative evaluation of socs-induced optical clearing efficiency of skull. Quant Imaging Med Surg. 5(1):136–142.